# Fractionation and Solution Properties of PS-*b*-PCEMA-*b*-P*t*BA Nanofibers

**Guojun Liu,* Xiaohu Yan, Xingping Qiu, and Zhao Li**

*Department of Chemistry, University of Calgary, 2500 University Drive, NW, Calgary, Alberta, Canada T2N 1N4*

*Received January 9, 2002*

ABSTRACT: Block copolymer nanofibers (BCNs) may be viewed as the macroscopic counterparts of polymer chains. While many techniques exit for the fractionation and characterization of polymer chains, these techniques generally fail when applied to BCNs. Reported in this paper is our preliminary success in fractionating polystyrene-*block*-poly(2-cinnamoyloxyethyl methacrylate)-*block*-poly(*tert*-butyl acrylate) or PS-*b*-PCEMA-*b*-P*t*BA nanofibers by centrifugation and in characterizing them by viscometry and dynamic light scattering (DLS).

## I. Introduction

Block copolymers self-assemble in bulk, forming various intricate nanometer-sized block segregation patterns.[1] Chemical processing of block-segregated copolymers has yielded various structures including nanospheres,[2] nanochannels in thin films,[3,4] and nanofibers.[5,6] To prepare nanofibers, Liu and co-workers[5] first used a polystyrene-*block*-poly(2-cinnamoyloxyethyl methacrylate) or PS-*b*-PCEMA sample containing hexagonally packed PCEMA cylindrical domains in the PS matrix. After photo-cross-linking of the PCEMA domains, nanofibers with PS hairs on their surfaces were obtained from dispersing the cross-linked cylindrical domains in solvents such as THF that solubilized the PS chains. More recently, ABC triblock copolymers have been used by Liu and co-workers to produce nanofibers and derivatives including nanotubes[7] and polymer/$Fe_2O_3$ superparamagnetic nanofibers.[8]

Structurally, BCNs may be viewed as the macroscopic counterparts of polymer chains. Illustrated in Scheme 1 is the structural comparison between a poly(*n*-hexyl isocyanate), PHIC, chain and a PS-*b*-PCEMA nanofiber.

In a PHIC chain, the backbone is made of imide units joined linearly and the hairs are -$(CH_2)_5CH_3$. Their counterparts in a PS-*b*-PCEMA nanofiber would be the cross-linked PCEMA cylinder and PS chains, respectively. While many techniques exist for the fractionation and characterization of polymer chains, the techniques generally fail when applied to BCNs. We have, for example, failed to fractionate BCNs by precipitation fractionation probably because there was little variation in polymer−solvent interaction parameter, $\chi$, from fiber to fiber. Gel permeation chromatography could not be used to fractionate or characterize the BCNs, because large BCNs could not be eluted out of the columns. Accurate molecular weight determination by light scattering using the Zimm-plot method was impossible because of the large size of the fibers.[5c] BCNs are, however, of tremendous interest either as a new entity of academic curiosity or as a potentially useful material. In this paper, we report our preliminary success in fractionating such fibers by centrifugation and in characterizing them by viscometry and DLS.

The fibers investigated here were prepared by following Scheme 2 from polystyrene-*block*-poly(2-cinnamoyloxyethyl methacrylate)-*block*-poly(*tert*-butyl acrylate) or PS-*b*-PCEMA-*b*-P*t*BA synthesized for another project

**Scheme 1. Structural Comparison between a PS-*b*-PCEMA Nanofiber and a PHIC Chain at Different Magnifications**

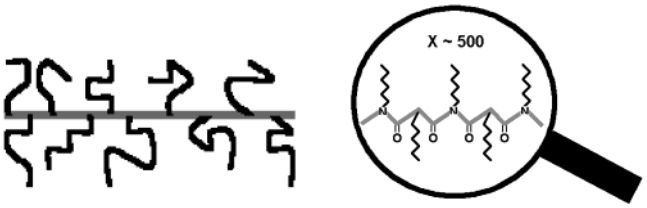


**Scheme 2**

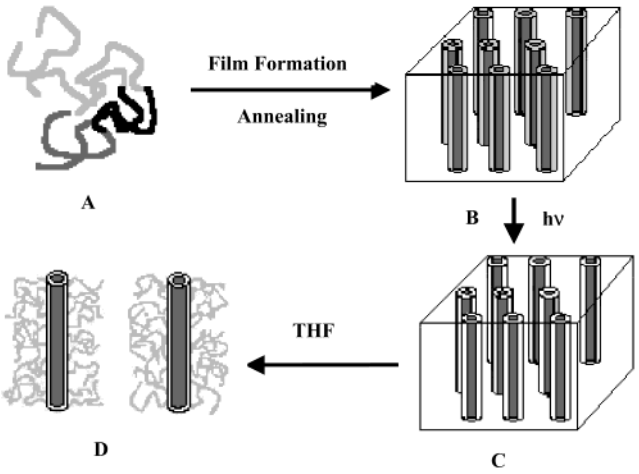


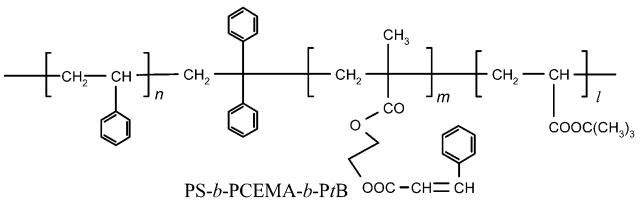


where $n = 560$, $m = 140$, and $l = 160$. In bulk films consisting of the triblock and a homo-PS (hPS) sample, PCEMA and P*t*BA formed concentric cylindrical domains dispersed in the continuous matrix of PS (**B**, Scheme 2). The PCEMA shells were then photo-cross-

10.1021/ma020038r CCC: $22.00 
Published on Web 08/21/2002

**Table 1. Characteristics of PS-*b*-PCEMA-*b*-P*t*BA**

| $dn_r/dc$ (mL/g) | LS $\bar{M}_w$ (g/mol) | GPC $M_w/\bar{M}_n$ | NMR $n/m/l$ | $n$ | $m$ | $l$ |
|---|---|---|---|---|---|---|
| 0.151[a] | $1.15 \times 10^5$ | 1.16 | 100/25/28 | 560 | 140 | 160 |

[a] Specific refractive index increment measured at 633 nm in THF. Light-scattering molar mass was determined in THF as well.

linked (**B** → **C**). Dispersing the cross-linked cylindrical domains in THF yielded isolated triblock copolymer nanofibers (**C** → **D**).

## II. Experimental Section

**Polymer Preparation and Characterization.** The preparation and characterization of PS-*b*-PCEMA,[9] PCEMA-*b*-P*t*BA,[10] and PS-*b*-PCEMA-*b*-P*t*BA[8] have been reported before and the procedures are thus not repeated here. Using the weight-average molar mass of $1.15 \times 10^5$ g/mol determined for the triblock from light scattering in THF and $n/m/l = 1.00/0.25/0.28$ determined from NMR, we obtained the average repeat units of 560, 140, and 160 for styrene, CEMA, and *t*BA, respectively. The other molecular characteristics of the polymer are summarized in Table 1.

**Nanofiber Preparation.** The detailed procedure for PS-*b*-PCEMA-*b*-P*t*BA nanofiber preparation has been reported.[8] It essentially involved mixing 100 parts, by weight, of the triblock with 30 parts of a homopolystyrene standard, $\bar{M}_w = 2500$ g/mol and $\bar{M}_w/\bar{M}_n = 1.09$. The mixture was then dissolved in toluene. Bulk films were obtained after toluene evaporation over 5 days. In such bulk films, the volume fraction for PS was 64.6%, and those for PCEMA and P*t*BA were 21.1% and 14.3%, respectively.[3c] The PCEMA and P*t*BA blocks formed concentric cylindrical domains dispersed in the continuous PS matrix, which was in agreement with that observed by Breiner et al.[11] for another triblock system. The films were then irradiated with a focused light beam, from a 500-W mercury lamp, that had passed a 290 nm cutoff filter to achieve a CEMA double bond conversion of 23%. The cross-linked cylinders were dispersed after dissolving the films in THF. The sample was first centrifuged at an acceleration of 170*g* for 10 min to remove insoluble gels. To separate the nanofibers from hPS, hexane, four times the volume of THF, was added to the supernatant. The mixture was centrifuged again at an acceleration of 170*g* for 10 min to settle the nanofibers. The yield of the nanofibers was 55%.

**Nanofiber Fractionation.** Nanofibers, ~220 mg, in 90 mL of THF were centrifuged at 1500*g* for 10 min. The precipitate was discarded. The rest of the sample was then centrifuged at 3290*g*, 7410*g*, and 13200*g*, respectively, each for 10 min to yield fractions 1, 2, and 3 as precipitate. Fraction 4 was obtained as the supernatant after centrifugation at 13200*g*. The amounts of solid obtained were 24, 43, 61, and 73 mg for fractions 1, 2, 3, and 4, respectively.

**Viscosity Measurement.** The nanofiber dispersions in THF were stirred overnight before their viscosities were measured using a modified Ubbelohde viscometer at 25 °C. The relative viscosity of a nanofiber solution was calculated using

$$\eta_r = t/t_0 \tag{1}$$

where $t$ and $t_0$ were the flow times for nanofiber solution and solvent, respectively. The validity of eq 1 demanded that no corrections were required of the kinetic energies of the flowing liquids. For this, we used a viscometer with a low linear average flow rate of ~10 cm/s. At this flow rate, the shear rate was ~1000 $s^{-1}$.[12]

**Dynamic Light Scattering.** The fractionated nanofiber samples were diluted with distilled and filtered THF to ~$5 \times 10^{-6}$ g/mL. After further centrifugation at 500*g* for 10 min, the sample was carefully transferred with a syringe, which was thoroughly rinsed with filtered THF, into a quartz cylindrical cell with a 25 mm diameter for measurement. At such a dilution, there was ~0.1 nanofiber in the volume $L^3$, where $L$, the average contour length of the nanofiber, was assumed to be ~5 $\mu$m for the calculation.

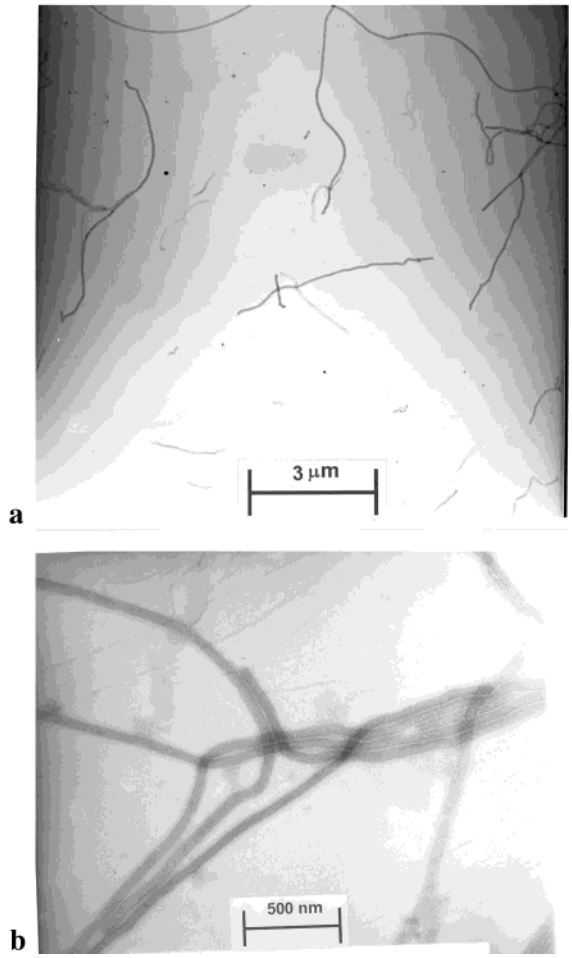


**Figure 1.** TEM images of nanofiber fraction 3 at different magnifications.

A Brookhaven 9025 instrument equipped with 10 mW He−Ne laser operating at 632.8 nm was used for DLS measurements. The BI-9000 AT digital autocorrelator used had 256 channels that were ratio spaced. The data were treated with software provided by Brookhaven to obtain the first cumulants or average decay rates $\bar{\Gamma}(q)$.

**TEM Studies.** TEM images were obtained using a Hitachi H-7000 instrument operated at 75 kV. TEM samples were obtained by aspirating a fine mist of a dilute solution (~0.1 mg/mL) of the polymer nanofibers onto a carbon-coated copper grid using a home-built device.[13] The samples were then placed in a vial containing osmium tetraoxide vapor for 4 h to stain the PCEMA double bonds.

## III. Results and Discussion

**Nanofiber Fractions.** We fractionated the nanofibers following procedures detailed in the Experimental Section. Illustrated in parts a and b of Figure 1 are the TEM images of nanofiber fraction 3 at different magnifications. All of the fibers seem to have a similar diameter.

To obtain length distributions, tens of TEM images were taken of each fraction. Each TEM image was then examined carefully to obtain the length of each fiber with discernible ends. After obtaining lengths for over 100 fibers for each fraction, the data were organized and presented in Figure 2. The data points in Figure 2 were evenly spaced with length intervals at 2 $\mu$m. The height $P(L_i)$ at $L_i$ denotes the relative population of fibers with

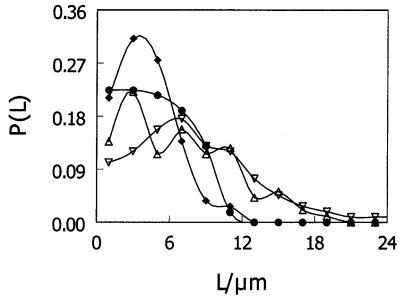


**Figure 2.** Plots of relative fiber population as a function of length for fractions 1 (▽), 2 (△), 3 (●), and 4 (◆).

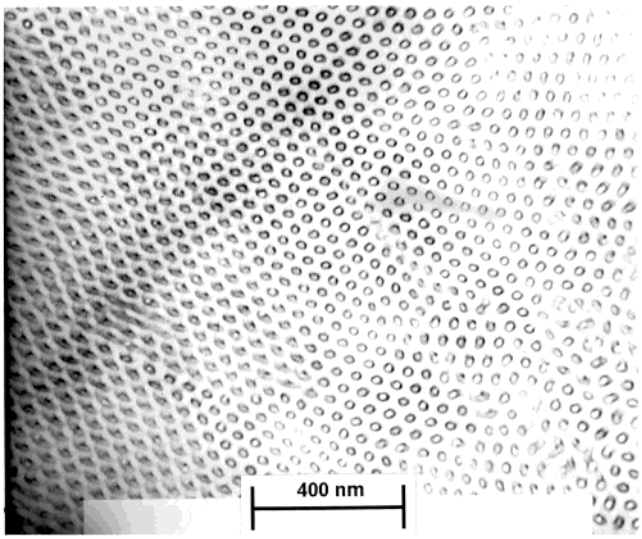


**Figure 3.** TEM image of a thin section of a PS-*b*-PCEMA-*b*-P*t*BA/hPS bulk film.

lengths between $(L_i - 1)$ and $(L_i + 1)$ $\mu$m. The raw data were also used to obtain the average lengths for the fractions. Averaging over 116 fibers, we obtained an average length of $4.7 \pm 2.8$ $\mu$m for fraction 3. Following a similar procedure, we obtained the average lengths of $7.8 \pm 5.1$, $6.7 \pm 4.0$, and $4.1 \pm 2.6$ $\mu$m for fractions 1, 2, and 4, respectively. The data of Figure 2 and the average nanofiber lengths clearly indicated that the fractionation worked. The longer fibers settled more readily, because the effective mass, which was the difference between the mass of the fiber and that of solvent replaced by it, increased with nanofiber length.[14]

The lengths $L$ thus determined were used to calculate the average molar masses $M_L$ of the nanofiber fractions using

$$M_L = N_A \pi L[\rho_B {r_B}^2 + \rho_C({r_C}^2 - {r_B}^2) + \rho_S({r_S}^2 - {r_C}^2)] \quad (2)$$

where $N_A$ is the Avogardro constant. $\rho_B = 1.02$, $\rho_C = 1.25$, and $\rho_S = 1.04$ g/mL are the densities of P*t*BA, PCEMA, and PS, respectively.[3c,5c] $r_B$, $r_C$, and $r_S$ are the radii of the P*t*BA core cylinder, the PCEMA shell cylinder, and the overall dry nanofiber, respectively.

The $r_B$ and $r_C$ values were obtained from Figure 3, a TEM image of a thin section of a PS-*b*-PCEMA-*b*-P*t*BA/hPS precursor film that was irradiated and dissolved to yield the nanofibers. The PCEMA domains appeared dark in this TEM image as PCEMA was selectively stained with $OsO_4$. Since the PCEMA and P*t*BA cylinders were small, we followed the approach of Breiner et al.[11] to determine $r_B$ and $r_C$ to minimize error. In this method, the average intercylinder distance, $L_c$, was determined from the TEM image first. The volume fractions of 14.3% and 21.1% for the P*t*BA and PCEMA blocks in the bulk film containing hPS and the $L_c$ value of 49.6 nm were then used to calculate $r_B$ and $r_C$. They were 9.8 and 15.5 nm, respectively. The radius $r_S$ for the dry PS-*b*-PCEMA-*b*-P*t*BA nanofibers containing no hPS was calculated to be 22.5 nm from $r_C$ and the volume fractions of PS, PCEMA and P*t*BA in the triblock. Inserting the $r_B$, $r_C$, and $r_S$ values into eq 2, we calculated a molar mass of $1.05 \times 10^{13}$ g for a 1.00-cm-long fiber. The number-average molar mass for each fraction was evaluated from this unit-length-fiber molar mass and the $L$ values listed in Table 2. The values were on the order of $10^9$ g/mol, and thus the fibers were indeed "suprapolymer chains".

**Dynamic Light Scattering Data.** Figure 2 provided direct evidence for nanofiber fractionation by centrifugation. The estimation of the average nanofiber lengths from TEM images was tedious and inaccurate. The precision deteriorated for fibers of greater lengths, as such fibers were entangled and many a time one could not tell the starting and finishing ends of a fiber. Then, the size of a sample examined by TEM was generally small and the statistical error could be large. Another independent technique confirming the effectiveness of the fractionation method was highly desirable. Because of the high molar masses of the nanofibers, we found out on a previous occasion[5c] that the determination of the molar masses by static light scattering using the Zimm plot method was impossible. Thus, we explored the use of dynamic light scattering for this purpose.

The scattered field autocorrelation function $g_1(q,t)$ deduced from the DLS raw data can always be treated by the cumulant method.[15] In the method of first cumulant, $g_1(q,t)$ is normalized and $\ln(g_1(q,t)/g_1(q,0))$ at short times is fitted by

$$\ln(g_1(q,t)/g_1(q,0)) = -\bar{\Gamma}(q)t + \ldots \quad (3)$$

where $q$ denotes the magnitude of the scattering wave vector; $\bar{\Gamma}(q)$, equal to $q^2\langle D\rangle$ or $q^2 D_a(q)$, is the average decay rate. Shown in Figure 4 is the variation in the apparent diffusion coefficient $D_a(q)$ calculated from $\bar{\Gamma}(q)/q^2$ for the nanofiber fractions plotted as a function of $q$ in the scattering angle range ~25 to ~130°. The solid lines represent curves drawn through the data for visual aid. The $D_a(q)$ values increase from fraction 1 to 2, 3, and 4 regardless of the $q$ value and confirm nanofiber fractionation by centrifugation.

**Treatment of DLS Data.** The determination of any nanofiber structural parameters from the DLS data required the use of a model. Figure 1 revealed that the dry nanofibers were wormlike or mostly straight with occasional kinks, which could have arisen from defects such as dislocations and grain boundaries in the original sphere packing. Alternatively, the kinks could have developed due to surface tension effect caused by solvent evaporation during TEM speciemen preparation or the nanofibers could have been rigid and straight in dilute solutions. Thus, the light-scattering data of the nanofibers should be treated by both the wormlike filament and the rigid rod model.

Assuming the decoupling between the rotational and translational motions, Pocora[16] was the first to work out the DLS $g_1(q,t)$ for optically isotropic thin rods with contour length $L$. For cases where the translational and rational motions are coupled because of anisotropy in the translational diffusion, the Pecora theory has been

**Table 2. Characteristics of the Nanofiber Fractions**

| fraction | TEM length ($\mu$m) | TEM molar mass ($10^{-9}$ g/mol) | [$\eta$] (mL/g) | $k'$ | $D_a(q\rightarrow\infty)$ ($10^{13}\times$ m$^2$/s) | $D_a(q\rightarrow 0)$ ($10^{13}\times$ m$^2$/s) | DLS length ($\mu$m) | DLS molar mass ($10^{-9}$ g/mol) |
|---|---|---|---|---|---|---|---|---|
| 1 | 7.8 ± 5.1 | 8.2 ± 5.4 | 231.1 ± 4.7 | −(0.39 ± 0.13) | 9.1 | 6.0 | 6.3 | 6.6 |
| 2 | 6.7 ± 4.1 | 7.0 ± 4.3 | 214.6 ± 1.7 | 0.15 ± 0.03 | 9.6 | 5.9 | 5.8 | 6.1 |
| 3 | 4.7 ± 2.8 | 4.9 ± 2.9 | 163.5 ± 1.2 | 0.28 ± 0.02 | 12.6 | 7.9 | 4.1 | 4.3 |
| 4 | 4.1 ± 2.6 | 4.3 ± 2.7 | 121.4 ± 13.8 | 0.71 ± 0.24 | 19.8 | 12.5 | 2.1 | 2.2 |

refined.[17−19] The rigid rod model has been successfully used to treat data obtained for tobacco mosaic virus,[20] collagen,[21] and fd virus[22] and even for cylindrical micelles of poly(ethylene oxide)-*block*-poly(propylene oxide)-*block*-poly(ethylene oxide).[23] Various theories including those by Reineker and co-workers[24] and Yamakawa and co-workers[25] also exist for treating the DLS data of wormlike chains. The wormlike chain model treats the best the DLS data of poly(*n*-hexyl isocyanate),[26] cylindrical micelles of low molar mass surfactants,[27] and DNA.[28] Treating DLS data with the rigid rod model generally allows the estimation of the rod length. The use of the wormlike chain model yields the chain persistence length.

A fundamental assumption of the two models is that the filament of interest is thin and possesses a uniform cross section. The criteria are definitely not met by our nanofibers. The diameter of the dry fibers is 45 nm and this $d$ value should be ∼80 nm for solvent-swollen fibers. The fibers possess a three-layer structure and are not optically isotropic across its diameter. Strictly speaking, none of the existing theories can be used to treat the DLS data of our nanofibers. We treated the DLS data applying the rigid rod model nonetheless just to see if we could extract reasonable lengths for the nanofibers. We did not attempt data treatment using the wormlike filament model for its mathematical complexity.

According to Maeda and Fujime,[17] the apparent diffusion coefficient of rigid rods in dilute solution satisfies

$$\bar{\Gamma}(q)/q^2 = D + (L^2/12)\Theta f_1(k) - \Delta[{}^1/_3 - f_2(k)] \quad (4)$$

where $k = qL$; $\Delta$, equal to $D_{\uparrow} - D_{\rightarrow}$, denotes the difference between the coefficients of diffusion of the rod parallel and perpendicular to the rod's axis; $\Theta$ is the rotational diffusion coefficient; and $D$, equal to $({}^1/_3)(D_{\uparrow} + 2D_{\rightarrow})$, is the overall translational diffusion coefficient of the rod. The $f_1(k)$ and $f_2(k)$ in eq 6 are complex functions of $k$. To obtain approximate analytical expressions for $f_1(k)$ and $f_2(k)$, we fitted the $f_1(k)$ and $f_2(k)$ data tabulated by Maeda and Fujime with various functional forms. Of the limited number of functional forms we tested, eqs 5 and 6 fitted the data the best.

$$f_1(k) = 0.4785[1 - \exp(-0.05443k)] + \frac{0.4679}{0.9225 + \exp\left(-\dfrac{k - 5.800}{1.298}\right)} \quad (5)$$

and

$$f_2(k) = 0.1703[\exp(-1.196\times 10^{-1}\,k) + \exp(-1.685\times 10^{-5}k)] - \frac{0.2631}{1.709 + \exp\left(-\dfrac{k - 4.976}{0.7942}\right)} \quad (6)$$

where $0 \le k \le \sim 5000$.

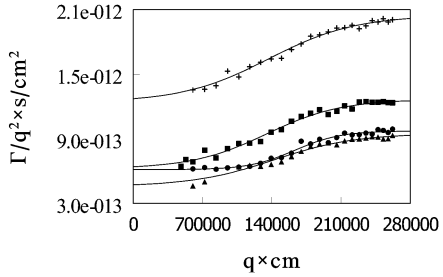


**Figure 4.** From bottom up, experimental $\bar{\Gamma}(q)/q^2$ vs $q$ data for fractions 1, 2, 3, and 4, respectively.

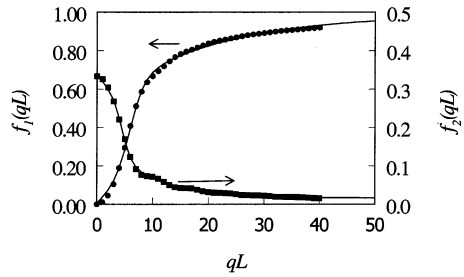


**Figure 5.** Best fits to $f_1(k)$ (●) and $f_2(k)$ (■) numerical data tabulated by Maeda and Fujime by eqs 5 and 6.

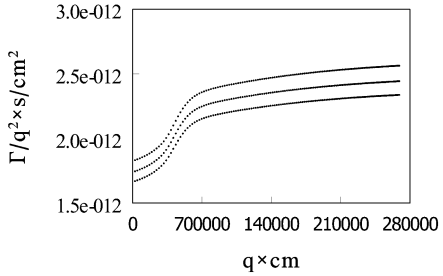


**Figure 6.** $\bar{\Gamma}(q)/q^2$ vs $q$ data generated from the Maeda and Fujime theory at $L = 1.5$ $\mu$m. From the top down, $d = 70$, 80, and 90 nm.

Various theoretical relations exist for calculating $D_{\uparrow}$, $D_{\rightarrow}$, and $\Theta$. They are functions of $d$ and $L$ only. Thus, $\bar{\Gamma}(q)/q^2$ vs $q^2$ data can be calculated from eq 4 making use of eqs 5 and 6 and those relating $D_{\uparrow}$, $D_{\rightarrow}$, and $\Theta$ to $d$ and $L$. We computed $\bar{\Gamma}(q)/q^2$ vs $q^2$ data using the Broersma[29,20] equations relating $D_{\uparrow}$, $D_{\rightarrow}$, and $\Theta$ to $d$ and $L$. The results are shown as a function of $d$ at $L = 1500$ nm in Figure 6 and as a function of $L$ at $d = 80$ nm in Figure 7. The general trend is that $\bar{\Gamma}(q)/q^2$ decreases with increasing $d$ and $L$. The $\bar{\Gamma}(q)/q^2$ data have a much stronger dependence on $L$ than $d$ with $\bar{\Gamma}(q)/q^2 \propto \ln(L/d)/L + const/L$.[28] Data of Figures 6 and 7 also show that $\Gamma(q)/q^2$ approaches constant values as $q \rightarrow 0$ and $q \rightarrow \infty$. In fact, $D_a(q\rightarrow\infty)/D_a(q\rightarrow 0) = 1.5$ for rods with $L/d \rightarrow \infty$. The low to high $D_a$ value transition occurs between $qL \approx 3$ and $qL \approx 10$ with the midpoint at $qL \approx 7$.

The experimental $\Gamma(q)/q^2$ data of Figure 4 seemed to follow the theoretical trend with $\Gamma(q)/q^2$ undergoing a low to high value transition. The transitions, however, occurred at $q$ values that were far too large to be reasonable for fibers with lengths given in Table 2. The

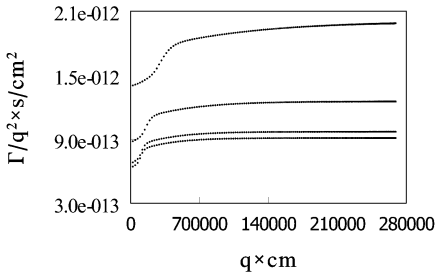


**Figure 7.** $\bar{\Gamma}(q)/q^2$ vs $q$ data generated from the Maeda and Fujime theory at $d = 80$ nm. From the top down, $L = 2.2$, 4.3, 6,1 and 6.6 $\mu$m, respectively.

discrepancy could be due to the invalidity of the rigid-rod assumption or the limitations of the model. At such a large $d$, Maeda and Fujime[17] argued explicitly that their theory would be valid only at large scattering angles, because the Rayleigh−Debye condition was not met at small scattering angles. Further deviation from theoretical results may be caused by the relative wide distribution in nanofiber lengths.

Because of the large $d$, we focused on comparing the generated and experimental $\bar{\Gamma}(q)/q^2$ data in the high $q$ region only. At $L$ = 6.3, 5.8, 4.1, and 2.1 $\mu$m, the generated $\bar{\Gamma}(q)/q^2$ data of Figure 7 compared well with the experimental data for fractions 1, 2, 3, and 4 shown in Figure 4 in the high $q$ region. These $L$ values were thus nanofiber lengths determined from DLS assuming the rigid-rod model. They agreed reasonably with the values of 7.8 ± 5.1, 6.7 ± 4.0, 4.7 ± 2.8, and 4.1 ± 2.6 $\mu$m determined from TEM. Thus, the rigid-rod model could at least be used to yield the **approximate** nanofiber lengths in this size range despite the large $d$ value. Efforts are being made to see if the rigid-rod model would work better for thinner diblock nanofibers.

**Intrinsic Viscosities.** For the polymer solution, the empirical Mark−Houwink relation[30]

$$[\eta] = KM^a \tag{7}$$

holds, where the constants $K$ and $a$ are positive. The intrinsic viscosity $[\eta]$ of polymer solution increases with polymer molar mass. We wondered if a similar relation would hold for BCN solutions.

Shown in parts a and b of Figure 8 are the $(\eta_r - 1)/c$ or $\eta_{sp}/c$ vs $c$ data for the four nanofiber fractions in THF. The solid lines represent the best fits to the experimental data by the empirical expression:

$$\eta_{sp}/c = [\eta] + k'[\eta]^2 c \tag{8}$$

where $k'$ is the Huggins coefficient.[30] The fitting parameters $[\eta]$ and $k'$ thus generated are presented in Table 2 together with their standard deviations.

The $[\eta]$ values of the nanofibers are comparable with those of solutions of linear polystyrene with a molar mass of $\sim 10^6$ g/mol.[31] The relatively low $[\eta]$ values of the fibers, compared with those of polymer chains on a similar molar mass basis, are in agreement with the trend observed for block copolymer micelles[32] and suggest more compact packing of polymer segments in the solvated nanaofibers than in linear polymer chains. The increase in $[\eta]$ from fraction 4 to fraction 1 suggests the possible validity of eq 7 and nanofiber fractionation by centrifugation.

**Huggins Coefficient *k′*.** For linear nonpolar polymer chains, $k'$ is normally between 0.30 and 0.50. $k'$ has been

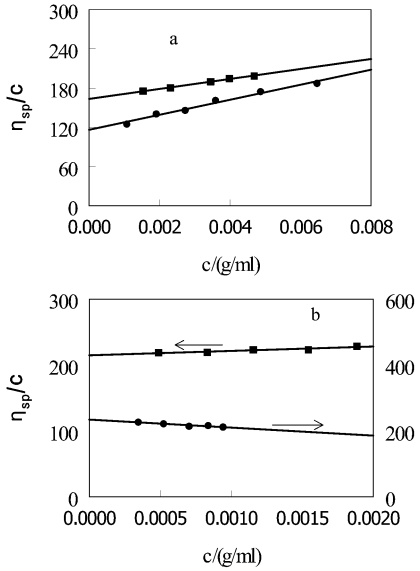


**Figure 8.** $(\eta - \eta_0)/\eta_0 c$ vs c plots for the nanofiber samples in THF. Data for fractions 3 (■) and 4 (●) are shown in Figure *a* and those for fractions 1 (●) and 2 (■) are shown in *b*.

observed to both increase and decrease slightly with the molar mass of polymer chains.[12,31] A similar $k'$ dependence on the molar mass has been established for wormlike chains including PHIC[33] and triple helixes of *Schizophyllum commune* polysaccharide.[34] Of all the data listed in the Polymer Handbook,[31] there was only one set of negative $k'$ values. The drastic decrease in $k'$ with temperature to negative values has been attributed to polymer chain conformation change with temperature in the original literature.[35]

Table 2 gives $k' = 0.71 \pm 0.24$ for fraction 4 of the nanofibers and $k' = -(0.39 \pm 0.13)$ for fraction 1. This drastic decrease in $k'$ with the molar mass and the negative $k'$ value for fraction 1 cannot be accounted for by possible experimental errors, as the standard deviations in $k'$ are relatively low.If the argument used in ref 35 can be borrowed at all, this abnormal $k'$ variation trend can be attributed to nanofiber conformation change with increasing length. Fibers shorter than their persistence length may be viewed as rigid rods. They are wormlike only when they are significantly longer than the persistence length. Another possible reason for the results could be due to the nonzero shear rate used in this study. Although a shear rate of $\sim 1000$ s$^{-1}$ should be of no concern to traditional polymer samples,[12] it might still induce nanofiber alignment. The ordering tendency may increase with the nanofiber length due to increased aspect ratio. Unfortunately, we do not have a rheometer and cannot examine the effect of varying shear rate on the viscosity of the nanofiber dispersions presently.

**Mark—Houwink Constants.** Illustrated in Figure 9 are the ln[$\eta$]-vs−ln $M$ plots for the nanofiber fractions. Using $L$ and thus $M$ determined from TEM, we obtained $a = 0.94 \pm 0.17$ and $\ln(K/(\text{mL/g})) = -(7.0 \pm 1.7)$ with a correlation coefficient equal to 0.93 for the nanofibers. For flexible polymer chains solubilized in a good solvent, the $a$ value approaches but is typically less than less 0.80.[30] The $a$ value approaches 2 for rigid rods. If the same $a$ scale can be used for the nanofibers, an $a$ value of 0.94 suggests wormlike behaviors for the nanofibers

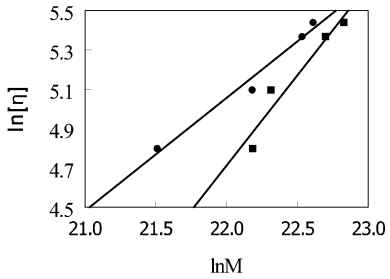


**Figure 9.** ln[$\eta$] vs ln $M$ plots for the nanofiber fractions. The molar masses were determined from TEM (■) and DLS (●), respectively.

in agreement with the TEM results. The large error of ±0.17 in the $a$ value, however, prevented us from concluding this unambiguously.

The $L$ and thus $M$ values determined from DLS were also used to yield a ln[$\eta$] vs ln $M$ plot with a correlation coefficient of 0.98. The resultant Mark−Houwink constants were $a = 0.58 \pm 0.06$ and $\ln(K/(\text{mL/g})) = -(3.3 \pm 0.6)$. The $a$ value of $0.58 \pm 0.06$ was close to 0.50 found for flexible chains in a Θ solvent and suggested high flexibility of the nanofibers in THF. This conclusion is most likely incorrect, as it is contradictory to what is shown in Figure 1. The wrong conclusion was reached probably because of error in $L$ determination by DLS assuming a rigid-rod filament model.

## IV. Conclusion

PS-*b*-PCEMA-*b*-P*t*BA nanofibers were fractionated by centrifugation. Longer fibers settled more readily probably because of their higher effective mass in a solvent. TEM, DLS, and viscometric studies of the fractionated nanofibers demonstrated the effectiveness of the fractionation method. Our viscometric study also showed that the Mark−Houwink empirical relation held for the suprapolymer chains, although an abnormal molar mass dependence was found for the Huggins coefficient. The Mark−Houwink constant $a$ determined using the intrinsic viscosities and the lengths, and thus the average molar masses of the nanofibers determined from TEM, suggested a wormlike structure for the nanofibers in THF. While the DLS data could be treated with the rigid-rod model to obtain the approximate lengths for the nanofibers, a more appropriate theory is required for treating such data quantitatively.

**Acknowledgment.** The NSERC of Canada is gratefully acknowledged for sponsoring this research.

## References and Notes

(1) See, for example: Bates, F. S. Fredrickson, G. H. *Phys. Today* **1999**, February issue, 32.
(2) Ishizu, K.; Onen, A. *J. Polym. Sci., A*: *Polym. Chem.* **1989**, *27*, 3719.
(3) a) Liu, G. J.; Ding, J.; Guo, A.; Herfort, M.; Bazett-Jones, D. *Macromolecules* **1997**, *30*, 1851. (b) Liu, G. J.; Ding, J. *Adv. Mater.* **1998**, *10*, 69. (c) Liu, G. J.; Ding, J.; Hashimoto, T.; Saijo, K.; Winnik, F. M.; Nigam, S. *Chem. Mater.* **1999**, *11*, 2233.
(4) a) Lee, J.-S.; Hirao, A.; Nakahama, S. *Macromolecules* **1989**, *22*, 2602. (b) Zalusky, A. S.; Olayo-Valles, R.; Taylor, C. J.; Hillmyer, M. A. *J. Am. Chem. Soc.* **2001**, *123*, 1519.
(5) a) Liu, G. J.; Qiao, L.; Guo, A. *Macromolecules* **1996**, *29*, 5508. (b) Liu, G. J. *Adv. Mater.* **1997**, *9*, 437. (c) Liu, G. J.; Ding, J.; Qiao, L.; Guo, A.; Gleeson, J. T.; Dymov, B.; Hashimoto, T.; Saijo, K. *Chem.−Eur. J.* **1999**, *5*, 2740.
(6) Massey, J.; Power, K. N.; Manners, I.; Winnik, M. A. *J. Am. Chem. Soc.* **1998**, *120*, 9533.
(7) a) Stewart, S.; Liu, G. J. *Angew. Chem., Int. Ed.* **2000**, *39*, 340. (b) Yan, X. H.; Liu, G. J.; Liu, F. T. *Macromolecules* **2001**, *34*, 9112.
(8) Yan, X. H.; Liu, G. J.; Liu, F. T.; Tang, B. Z.; Peng, H.; Pakhomov, A. B.; Wong, C. Y. *Angew. Chem., Int. Ed.* **2001**, *40*, 3593.
(9) Guo, A.; Tao, J.; Liu, G. J. *Macromolecules* **1996**, *29*, 2487.
(10) Henselwood, F.; Liu, G. J. *Macromolecules* **1997**, *30*, 488−493.
(11) Breiner, U.; Krappe, U.; Abetz, V.; Stadler, R. *Macromol. Chem. Phys.* **1997**, *198*, 1051.
(12) Moore, W. R. In *Progress in Polymer Science*; Jenkins, A. D., Ed.; Pergamon Press: Oxford, England, 1969; Vol. 1, p 1.
(13) Ding, J.; Liu, G. J. *Macromolecules* **1999**, *32*, 8413.
(14) See, for example, Williams, J. W. *Ultracentriguation of Macromolecules*; Academic Press: San Diego, CA, 1972.
(15) Berne, B. J.; Pecora, R. *Dynamic Light Scattering with Applications to Chemistry, Biology, and Physics*; Dover Publications: Mineola, NY, 2000.
(16) Pecora, R. *J. Chem. Phys.* **1968**, *48*, 4126.
(17) Maeda, T.; Fujime, S. *Macromolecules* **1984**, *17*, 1157.
(18) Kubota, K.; Urake, H.; Tominago, Y.; Fujime, S. *Macromolecules* **1984**, *17*, 2096.
(19) Wilcoxon, J.; Schurr, J. M. *Biopolymers* **1983**, *22*, 849.
(20) a) Wilcoxon, J.; Schurr, J. M. *Biopolymers* **1983**, *22*, 849. (b) Wada, A.; Ford, N. C.; Karasz, F. E. *J. Chem. Phys.* **1971**, *55*, 1798. (c) Schaeffer, D. W.; Benedek, G. B.; Schofield, P.; Bradford, E. *J. Chem. Phys.* **1971**, *55*, 3884.
(21) Claire, K.; Pecora, R. *J. Phys. Chem. B.* **1997**, *101*, 746.
(22) Newman, J.; Swinney, H. L. *J. Mol. Biol.* **1977**, *116*, 593.
(23) Lehner, D.; Lindner, H.; Glatter, O. *Langmuir* **2000**, *16*, 1689.
(24) Harnau, L.; Winkler, R. G.; Reineker, P. *J. Chem. Phys.* **1996**, *104*, 6355.
(25) Yoshizaki, T.; Osa, M.; Yamakawa, H. *J. Chem. Phys.* **1997**, *106*, 2828.
(26) Yoshida, N.; Yoshizaki, T.; Yamakawa, H. *Macromolecules* **2000**, *33*, 3254.
(27) Berlepsch, H. V.; Harnau, L.; Reineker, P. *J. Phys. Chem. B.* **1998**, *102*, 7518.
(28) Schurr, J. M. *Biopolymers* **1983**, *22*, 2207.
(29) a) Broersma, S. *J. Chem. Phys.* **1960**, *32*, 1626. (b) Broersma, S. *J. Chem. Phys.* **1960**, *32*, 1632. (c) Broersma, S. *J. Chem. Phys.* **1981**, *74*, 6989.
(30) See, for example, (a) Elias, H. G. *An Introduction to Polymer Science*; VCH: Weinheim, Germany, 1997. (b) Sperling, L. H. *Introduction to Physical Polymer Science*; John Wiley & Sons: New York, 1992.
(31) Brandrup, J.; Immergut, E. H. *Polymer Handbook*, 3rd ed.; John Wiley & Sons: New York, 1989; p VII 184.
(32) Tuzar, Z.; Kratochvil, P. *Surf. Colloid Sci.* **1993**, *15*, 1.
(33) Kuwata, M.; Murakami, H.; Norisuye, T.; Fujita, H. *Macromolecules* **1984**, *17*, 2731.
(34) Yanaki, T.; Norisuye, T.; Fujita, H. *Macromolecules* **1980**, *13*, 1462.
(35) Olayemi, J. Y. *Makromol. Chem.* **1982**, *183*, 2547.

MA020038R